RSC Advances

ROYAL SOCIETY OF CHEMISTRY

www.rsc.org/advances

Reaction mechanism of "Amine-Borane Route" towards Sn, Ni, Pd, Pt nanoparticles

Ortal Lidor-Shalev and David Zitoun

Department of Chemistry, Bar Ilan Institute of Nanotechnology and Advanced Materials (BINA), Bar Ilan University, Ramat Gan. 52900, Israel

Abstract

The understanding of the chemical reaction yielding to nanomaterials is often based on basic assumptions and novel syntheses are usually presented without knowledge on their reaction mechanism. Herein, the chemical reduction of metal precursors by *Lewis* complexes of amine-borane is fully investigated, reaction and mechanism, for the synthesis of metallic nanoparticles (NPs). In this study, Sn NPs are obtained by the chemical reduction of tin acetylacetonate complex [$Sn(acac)_2$] using dimethylamine-borane (DMAB) as a reducing agent. The reaction yields single crystalline Sn NPs indepentanly of the use of surfactant. The size of the NPs can be adjusted by regulating the complex/DMAB ratio. The use of DMAB as a reducing agent is extended to the synthesis of Ni, Pd, Pt and Sn/Pd NPs. We investigate the synthetic mechanism by using ^{11}B-NMR and calorimetric analytical tools. The mechanism is found to be specific to the acetylacetonate complexes and involves the reaction of borane on the ligand.

Introduction

The synthesis of metallic nanoparticles (NPs) has been extensively investigated for two decades and the demand for new reduction paths have increased in the last years. The hydrogen-rich Lewis complex ammonia-borane (AB; $BH_3{\cdot}NH_3$)[1,2] and its derivatives[3] are considered as a solid source for in-situ hydrogen generation . The AB complex is non-explosive, nontoxic, and an environmentally safe material. Moreover, AB compounds and their derivatives have been considered as potential materials hydrogen storages[4] and for fuels[5]. A derivative of AB, borane-dimethylamine complex (DMAB; $BH_3{\cdot}NH(CH_3)_2$), and its dehydrogenation/dehydrocoupling in the presence of catalysts [6, 7,8,9], such as Rh [10,11,12,13,14], Ni [15], Ti [16,17], Re[18], Pt[19], Pd[20] and Ir[21,22] have been investigated. Catalytic dehydrogenation of B-H bonds is an easy source for hydrogen (H_2) molecules that sequentially can reduce complexes to obtain metallic NPs.

Research on Sn NPs is not very common compared to noble metals, since it is hard to control the surface properties of the NPs. The synthesis of Sn NPs is relatively complicated, mainly due to the need for strong reducing agent or very reactive metal-organic precursors. Tin and tin oxide (SnO_2) NPs and bimetallic systems can be obtained by different methods[23,24,25]. However, some of those methods may lead to particle coalescence and growth. The most appropriate chemical method for obtaining relatively small crystalline Sn NPs is the chemical reduction of organometallic or metal-organic precursors in the presence of surfactants. The demand for Sn and SnO_2 NPs is mainly for MOS (metal-oxide semiconductor) hydrogen sensors and as anodic material for Li-ion batteries[26,27].

In this article, we propose to combine the use of a simple metal-organic precursor ($Sn(acac)_2$)) with amine-borane (AB) in the absence of surfactants. The importance of our synthesis is the ability to use a derivative of AB as a source for hydrogen molecules in a redox reaction leading to metallic NPs. In this research we report a new synthetic path for the synthesis of Sn NPs, with various sizes, by reducing metal precursors using DMAB as a reducing agent for obtaining the crystalline Sn NPs. The new route enables formation of Sn NPs with a thin oxide layer on their surface that have a tremendous advantage of a clean surface without using stabilizing ligands. Different conditions, such as time, concentration, surfactants, temperature, metal-organic precursor and reducing agent, influence the obtained Sn NPs and affect the yield. Various parameters are changed to obtain Sn NPs with a high homogeneity, a small size distribution, a stable colloidal system, a defined shape, and a clean surface. The same method, with DMAB as the reducing agent, is used in order to obtain monometallic and bimetallic assemblies of colloids. The use of DMAB as a reducing agent is extended to the formation of Ni, Pd, Pt and Sn_Pd NPs. In addition, the synthesis mechanism is investigated by analytical tools, like calorimetry and NMR spectroscopy.

Results

Optimization of Sn NPs synthesis conditions

The chemical reduction of $Sn(acac)_2$ as a metal-organic precursor with DMAB yielded Sn NPs in a surfactant free reaction. The best results in terms of clean surface, stable dispersion, low NPs aggregation, and relatively homogenous size, were achieved by the use of DMAB/$Sn(acac)_2$ ratio of 1:4. The Sn NPs colloidal dispersion was analyzed by TEM, XRD and DLS.

TEM images show the round morphology of the obtained Sn NPs from a stable DMSO colloidal solution (Figure 1a) with the occurrence of faceted nanoparticles (mainly cubic). Selected area electron diffraction (SAED) shows highly crystalline NPs with typical planes of *Tetragonal* Sn (Figure 1a inset), following the bulk tetragonal structure of Sn (JCPDS # 04-0673). The crystalline

structure is supported by powder X-ray diffraction (XRD) results with the *Tetragonal* cell parameters; a=b= 5.831Å, c=3.181Å (Figure 1b). No other phase, by-products, or crystalline oxides were observed, demonstrating the selectivity of the reaction.

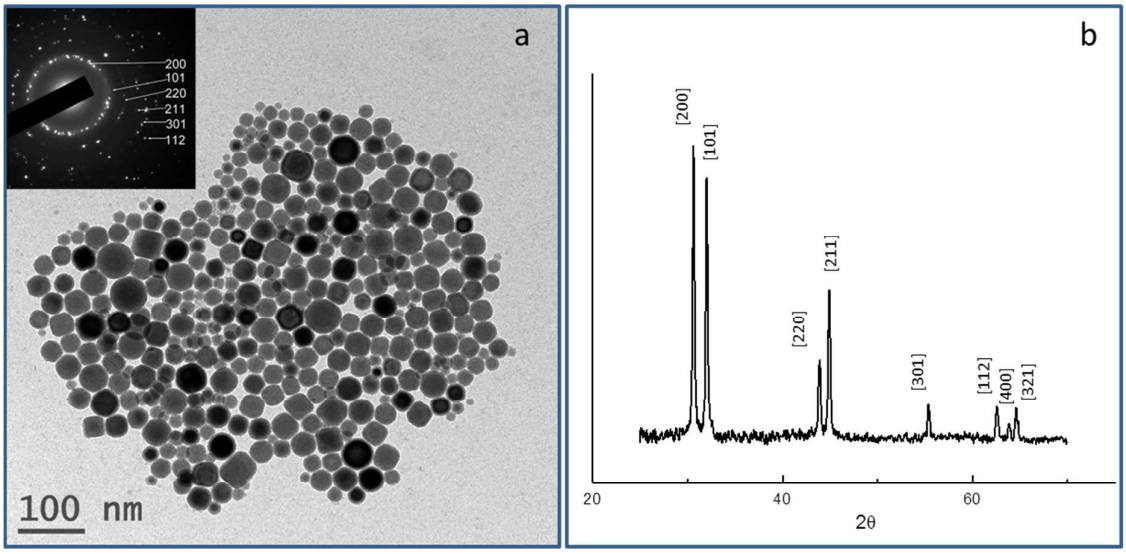

Figure 1: (a) TEM images of Sn nanoparticles with 1:4 ratio $Sn(acac)_2$ /amine-borane (inset: SAED) and (b) Powder X-Ray Diffraction

HRTEM of single nanoparticle reveals the single crystalline nature of the particles within a tetragonal phase (Figure 2A). The NPs surface is covered with a thin amorphous layer with a thickness of 3.7±1nm (Figures 2a). X-Ray Photoelectron spectroscopy (XPS) of the nanoparticles at the Sn edge $3d_{5/2}$ can be fitted with a main component (91%) centered at 486.8 eV (Sn^{IV}) and a minor component (9%) at 484.7 eV (Sn^0) (Figure S1). Such a spectrum is typical of metallic tin with an SnO_2 oxide shell. The Sn NPs have a spherical shape with a few square particles and some faceted ones (Figure 2c). The XPS results are supported by energy dispersive X-ray spectroscopy (EDS) (Figures S2b and S2c) of a single nanoparticle (Figure S2a). The EDS results show an increase of oxygen/tin atomic ratio from the core to the shell of the nanocrystal.

The Sn NPs polydispersity and the NPs mean size (37 ± 13 nm) were analyzed according to TEM images based on a statistical analysis of more than 200 NPs (Figure 2d). In addition to the NPs mean size from TEM, the size of the colloids in DMSO dispersion was measured by dynamic light scattering (DLS) and shows size distribution of a Gaussian centered at 37 nm and a secondary peak at 225 nm (Figure 2b). The main distribution of hydrodynamic diameters corresponds to the nanocrystal size distribution calculated from TEM images. The secondary peak may originate from the aggregation of the NPs that might occur in the absence of surfactants.

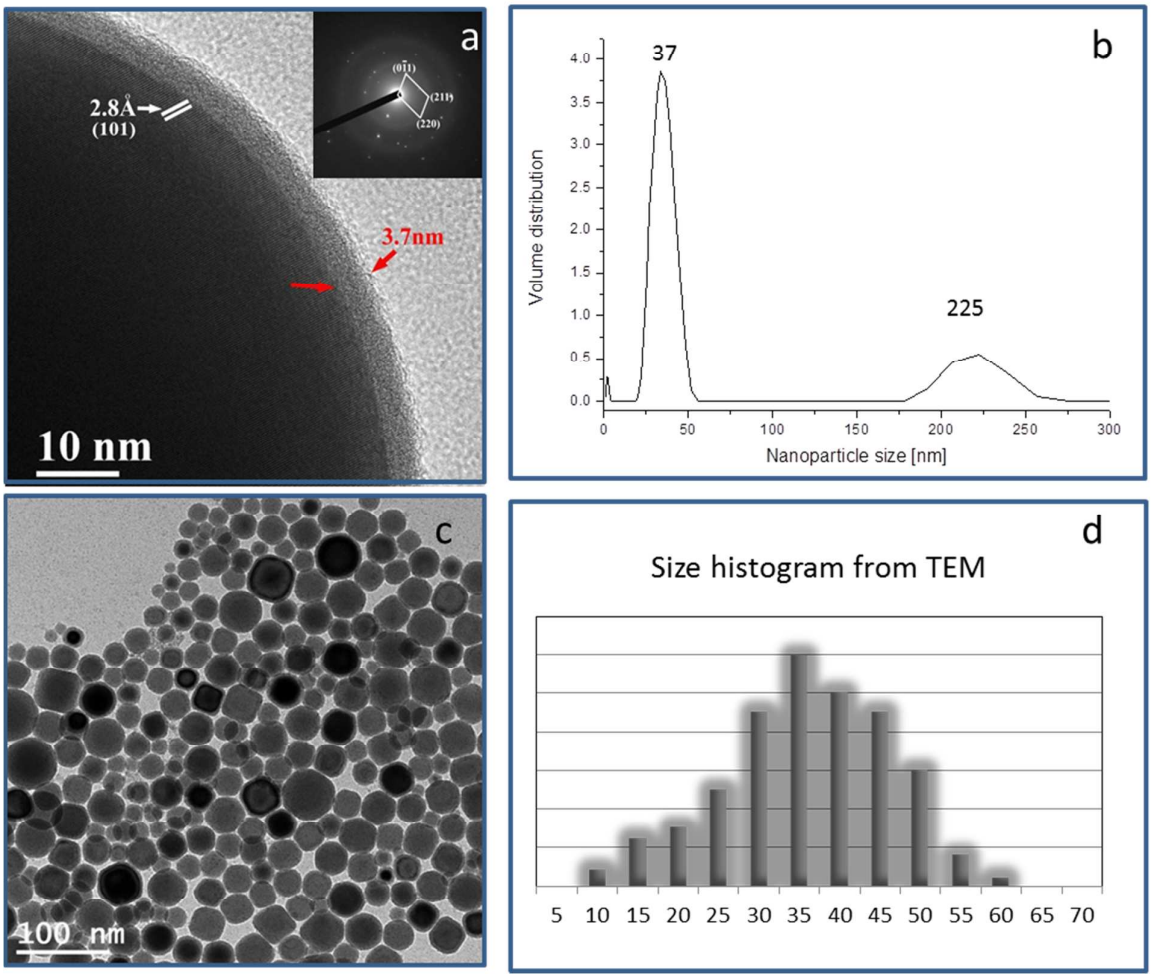

Figure 2: (a) HRTEM on a single nanocrystal, with the corresponding SAED (b) Particle size distribution from Dynamic Light Scattering, (c) TEM image of Sn nanoparticles, (d) Size histogram from TEM analysis.

Size control: Ratio between the precursor and DMAB

The ratio reducing agent/precursor influences the NPs size (Figure 3a-d). Increasing the ratio between the reducing agent (DMAB) and the metal precursor [$Sn(acac)_2$] yields larger average size and broader size distribution (Figure 3e). The exact stoichiometry for the amine-borane complex should be two equivalent of the metal precursor. Indeed, for such a ratio $Sn(acac)_2$ /amine-borane 1:2, the reaction yields Sn NPs with an average size of 17±9 nm. An excess of amine-borane complex leads to a quasi-linear increase of mean particle size, up to 90±20 nm for a ratio $Sn(acac)_2$ /amine-borane 1:12.

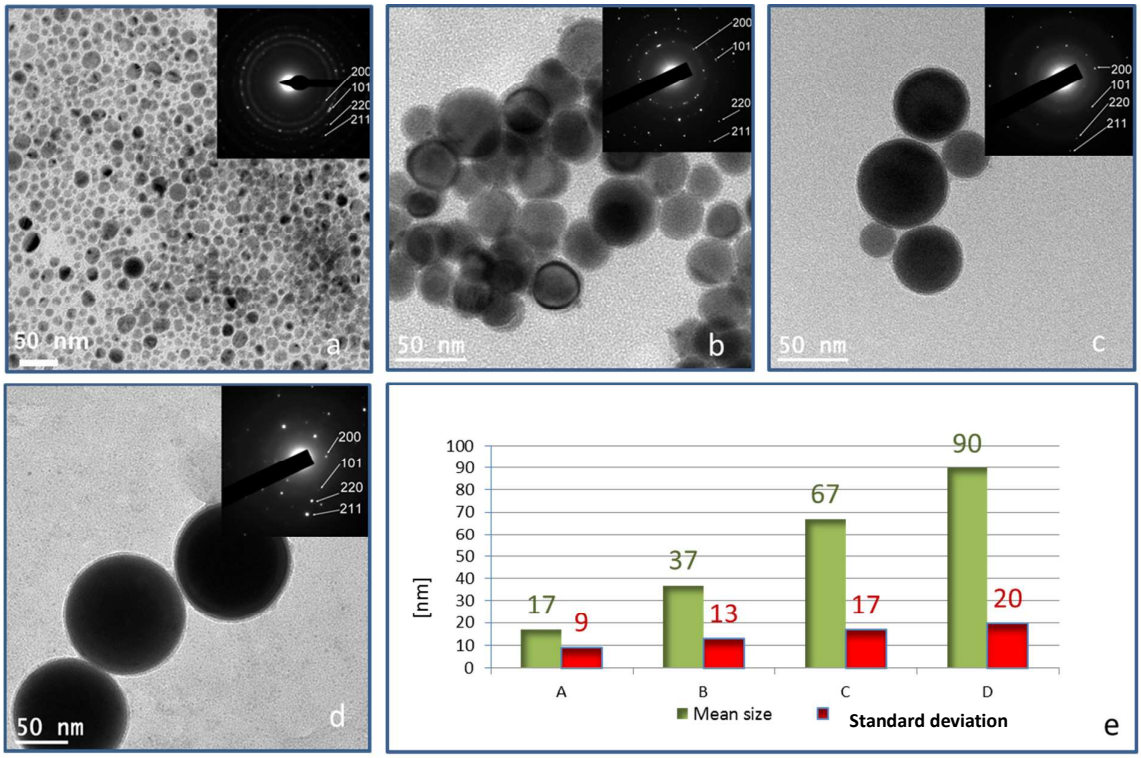

Figure 3: TEM images of Sn nanoparticles with different ratios $Sn(acac)_2$ /amine-borane : (a)1:2, (b)1:4, (c)1:8, (d) 1:12 and (e) Mean size and standard deviation.

The effect of steric surfactant on the NP size deviation

A steric stabilizer can improve the monodispersity of the particles. The surfactant hexadecylamine HDA is a steric stabilizer which usually controls the nanoparticle growth. After synthesis and purification, the colloids are dispersed in DMSO and the surfactant is washed out. Increasing the ratio surfactant/precursor slightly decreases the standard size deviation (Figure 4a-d). The presence of HDA does not influence the crystallinity of the NPs and has not a significant effect on the mean particle size.

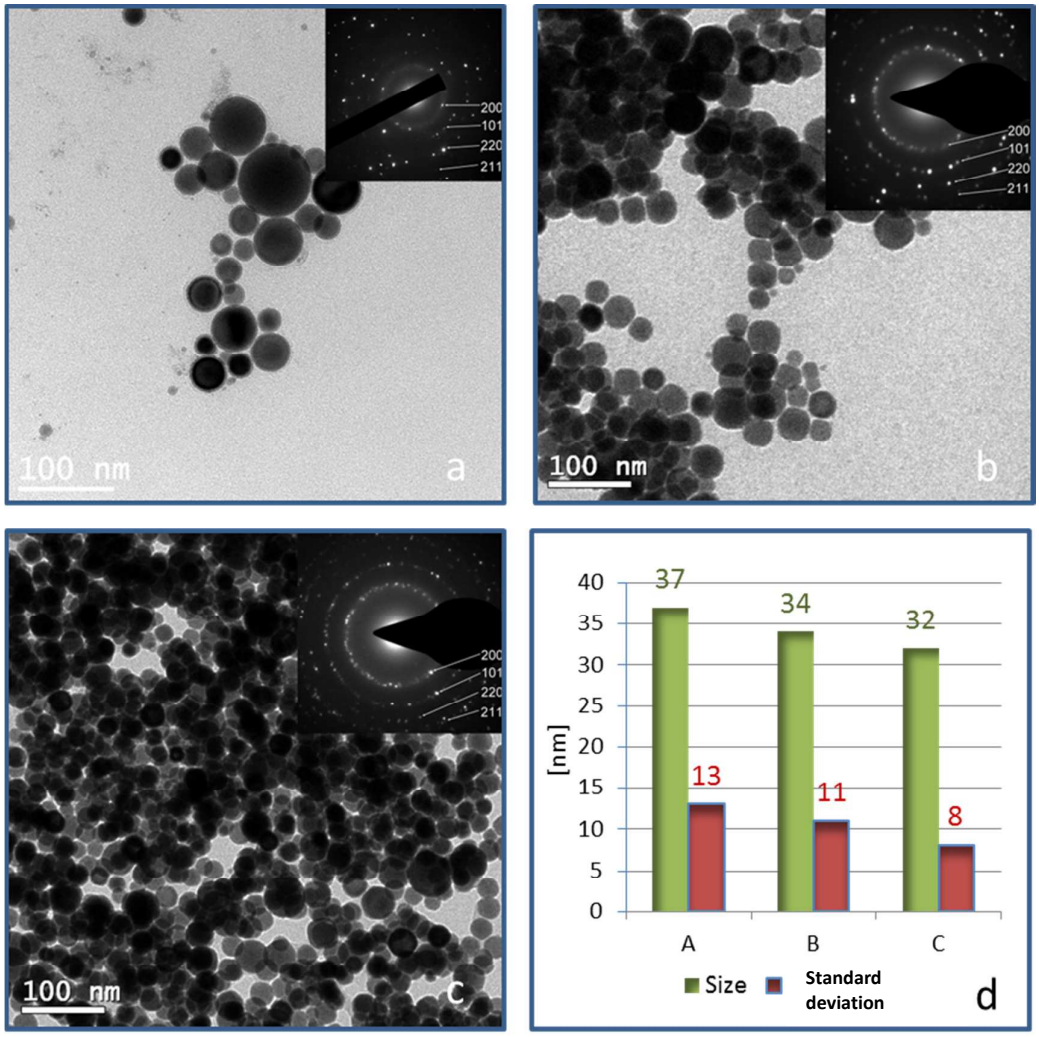

Figure 4: TEM images of Sn nanoparticles with a constant ratio $Sn(acac)_2$ /amine-borane ¼ and different metallic precursor/surfactant ratios: (a)no HDA,(b) 1:2, (c)1:4 and (d) mean size and standard deviation for the three batches.

Additional conditions for controlling NP size:

Different conditions were changed for further understanding the reaction mechanism. The reaction with $Sn(acac)_2$ starts after 25 minutes with a color change from light yellow to dark brown. The metal-organic complex $Sn(hfac)_2$ was chosen as a Sn(II) precursor with properties slightly different from $Sn(acac)_2$. The main change occurs from the electronegative CF_3 groups, which weakens the coordination to tin. As a consequence, the reaction is much faster in the same conditions of temperature and concentrations, yielding crystalline Sn NPs after 5 minutes only (Figure 5a).

Further reaction until 15 minutes does not increase the particle size or modify the size dispersion (Figure 5b).

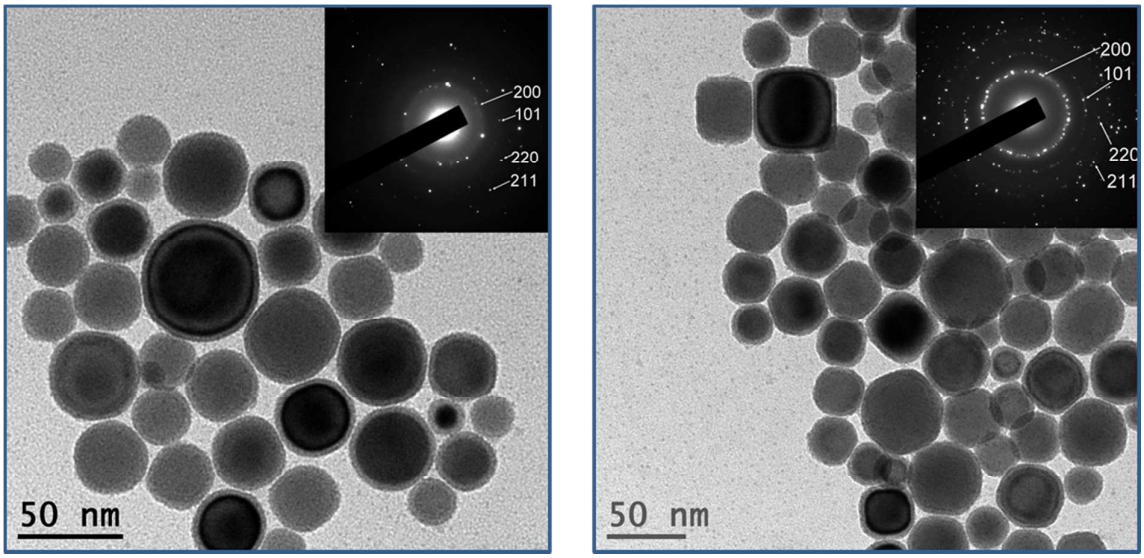

Figure 5: TEM images of a rapid reaction by using $Sn(hfac)_2$ as a precursor for obtaining Sn NPs [ratio $Sn(hfac)_2$/amine-borane 1:2], after different reaction times: (a) 5 min and (b) 15min.

Mechanism

A significant and important question mark remains on the reaction mechanism. In order to investigate the mechanism, we used ^{11}B-NMR spectra and DSC measurements. The ^{11}B-NMR spectra of different inorganic materials were reported in the literature[28,29]. The ^{11}B chemical shift of the starting reagent DMAB is -14.63 ppm (q, $^{1}J_{BH}$ = 96 Hz) (Figure 6a). The thermal decomposition product of DMAB shows a quartet at -13.30 ppm (q, $^{1}J_{BH}$ = 96 Hz) and a triplet at 5.60ppm (t, $^{1}J_{BH}$ = 113 Hz) is attributed to the cyclic dimer (Figure 6b). The by-product of the reduction by DMAB shows two signals in the ^{11}B-NMR spectrum: one typical of DMAB at -13.80 ppm (q, $^{1}J_{BH}$ = 97 Hz) and a singlet at 18.50 ppm which is attributed to a by-product containing a boron-oxygen chemical bond (Figure 6c). This singlet is attributed later to a dioxaborine complex. With one equivalent of DMAB, the only observed peak is the singlet at 18.51ppm, with no leftover DMAB (Figure 6d).

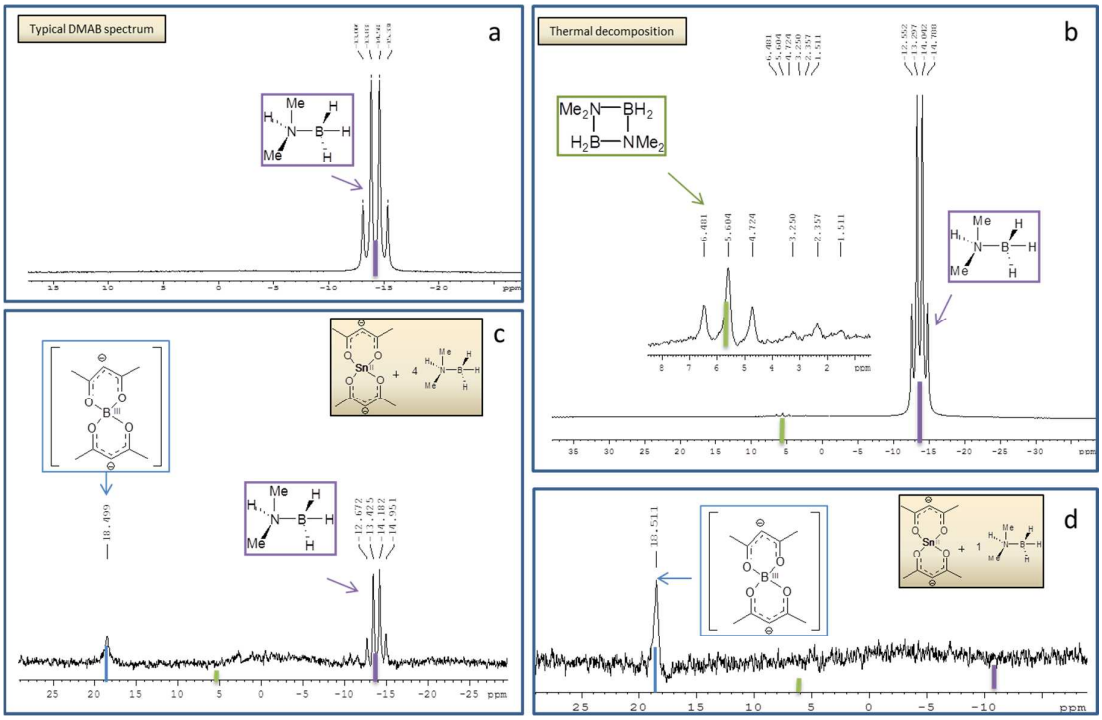

Figure 6: ^{11}B NMR (128 MHz, Chloroform) spectra of (a) DMAB, (b) DMAB after heating at 200 °C, (c) supernatant after reaction with ¼ equivalent of $Sn(acac)_2$ (d) and reaction with 1 equivalent of $Sn(acac)_2$.

The DSC curves on the pristine DMAB (Figure 7a) show an endotherm at 36°C (melting point) and at 164°C (boiling point), all in accordance with the literature [30,31]. An exotherm can be observed almost at the same temperature (around 160°C) which accounts for the formation of a DMAB dimer with H_2 release, as already observed from NMR and reported in the literature[32]. The same procedure is now applied to a mixture of DMAB with $Sn(acac)_2$. DSC results of different DMAB/$Sn(acac)_2$ ratios are shown (Figure 7, graphs b-d). The spectra do not display any endotherm and the main exotherm at 70°C is attributed to the reaction between $Sn(acac)_2$ and DMAB, yielding Sn NPs.

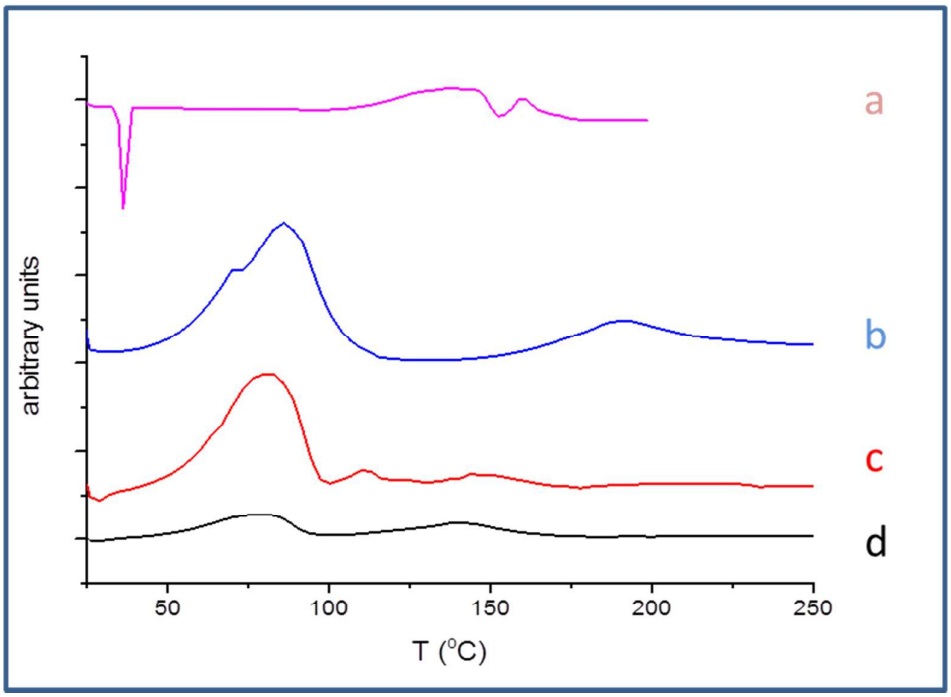

Figure 7: Differential Scanning Calorimetry (DSC) measurements of (a) DMAB, (b) $Sn(acac)_2$/DMAB 1:4 ratio, (c) $Sn(acac)_2$/DMAB 1:2 ratio and (d) $Sn(acac)_2$/DMAB 1:1 ratio.

Additional metallic NPs

The use of DMAB as a reducing agent was extended for the syntheses of additional metallic NPs. We succeeded to obtain Ni, Pd, Pt NPs and Sn/Pd bimetallic system (Figure 8). The chemical reduction of $M(acac)_2$ by DMAB [M=Ni, Pd, Pt] was found appropriate for the synthesis of FCC NPs with a small mean diameter (below 10nm). $Ni(acac)_2$ yield crystalline Ni NPs of 5±2 nm with a crystalline structure corresponding to the bulk (JCPDS # 04-0850; Fm-3m, a= 3.5238 Å). $Pd(acac)_2$ yield crystalline Pd NPs of 8±5 nm with a crystalline structure corresponding to the bulk (JCPDS # 05-0681; Fm-3m, a= 3.8902 Å). $Pt(acac)_2$ yield crystalline Pt NPs of 5±3 nm with a crystalline structure corresponding to the bulk (JCPDS # 04-0802; Fm-3m, a= 3.9231 Å). The crystallographic phases are confirmed by powder X-Ray Diffraction in the case of Pt and Pd, while Ni shows poor crystallinity (Figure S3).

Sn/Pd precursors yield crystalline Sn NPs of 45±9 nm with a crystalline structure corresponding to the bulk tetragonal Sn and crystalline Pd NPs of 5±1 nm with a crystalline structure corresponding to the bulk FCC Pd. The reaction with two different precursors yields two distributions of colloids which obviously correspond to large particles of Sn and small particles of Pd. No intermetallic phase can be observed, certainly due to the low temperature of reaction. Such an approach allows

for the decorrelation of the two reactions and could be extended to several bi-metallic systems. The only prerequisite seems to be the use of acetylacetonate complex.

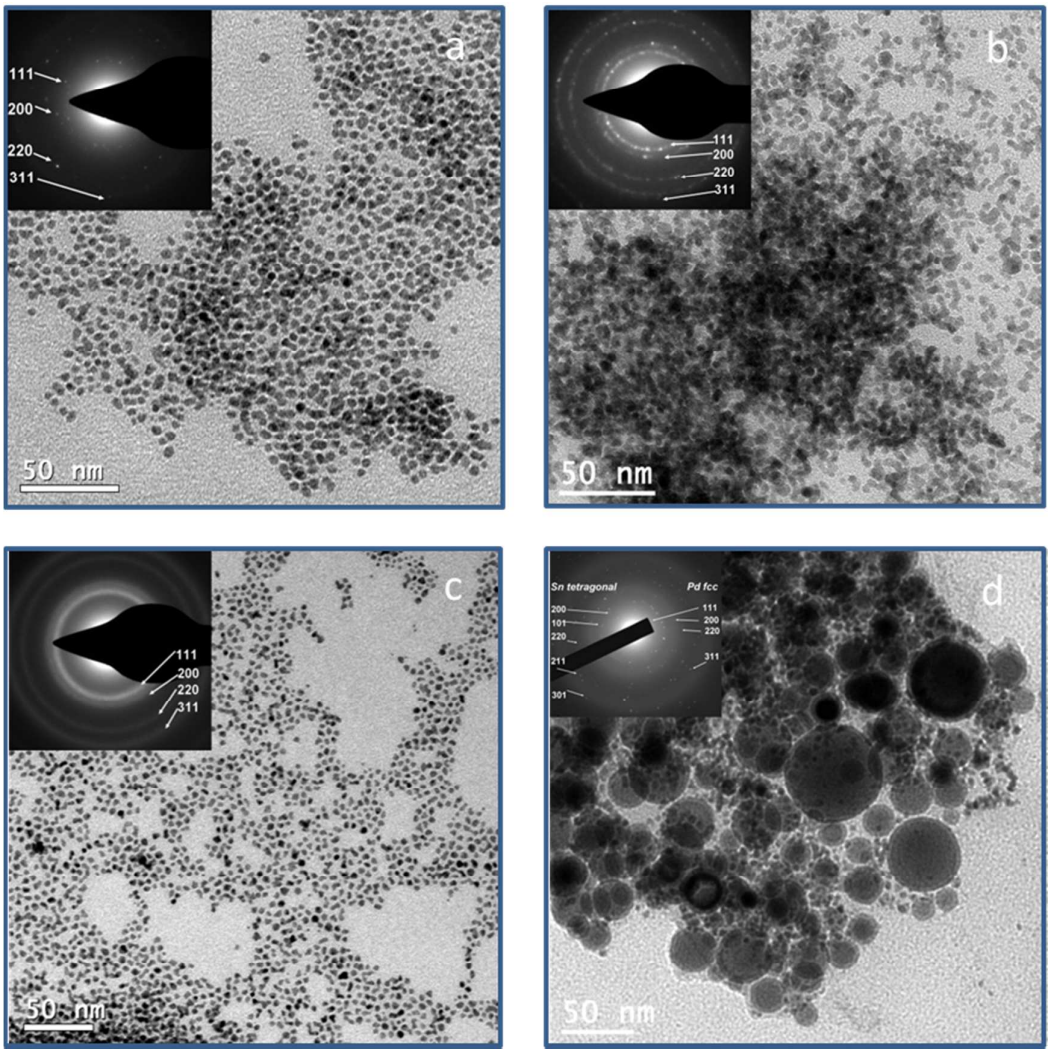

Figure 8: TEM images of Ni, Pd, Pt and Sn/Pd nanoparticles from $M(acac)_2$ and DMAB: (a) $Ni(acac)_2$ precursor, (b) $Pd(acac)_2$ precursor (c) $Pt(acac)_2$ precursor and (d) $Sn(acac)_2$ followed by $Pd(acac)_2$ precursors. Insets show the corresponding SAED.

Discussions

A new synthetic path of the chemical reduction of metal-acetylacetonate complexes by amine-borane complex (AB) was investigated and the results displayed in the section below. In the case of

Sn, the NPs mean diameter and size distribution can be controlled by the metal precursor/reducing agent ratios with diameters in the range of 15 to 90 nm. The mean size increases almost linearly with the molar ratio between amine-borane and $Sn(acac)_2$. As a consequence, if we assume a nucleation-growth model typical for colloidal nanoparticles synthesis, the kinetics seem to be controlled by the growth step and not by the nucleation step. Indeed, a nucleation controlled reaction would give the opposite trend with smaller NPs resulting from higher amount of AB.

The standard deviation remains low even for large particles, in the range of 30%. This result is noticeable for NPs synthesized in the absence of surfactants, which are usually the main pathway towards low polydispersity. The addition of hexadecylamine as steric surfactant improves the size deviation without a significant change in the mean diameter (Fig. 4). We assume that hexadecylamine can limit the particle size growth by the stronger affinity to NPs, as previously demonstrated on Sn NPs.

In all cases, the particles are suspended in a polar solvent after washings; DMSO displays the best dispersion as the electrostatic repulsion stabilizes the colloidal solution. The use of a steric stabilizer is not necessary and the DMSO dispersions are stable for weeks.

In this research, $Sn(acac)_2$ is used as a metal-organic precursor to yield Sn NPs in combination with amine-borane complexes. Such a combination has not been reported before. Other complexes with dimethylamine moieties have been thorough fully investigated by Chaudret et al for the syntheses of Sn and SnO_2 NPs from $\{Sn(NMe_2)_2\}_2$ metal-organic precursors. Sn/SnO_2 NPs in the range 10-20 nm are obtained by the thermal decomposition of $\{Sn(NMe_2)_2\}_2$, followed by a controlled surface hydrolysis and finally oxidation to SnO_2[33,34]. The homoleptic Sn(II) amides have been singled as metal precursors because of the relative thermodynamic weakness of the Sn-N bond $\{Sn(NMe_2)_2\}_2$ which enables reactivity even at low temperature. Noteworthy, the dimethylamine moiety resembles the Lewis base in the amino-borane complex. Therefore, the reaction we propose is an alternative to the synthesis of Sn(II) amide complexes with a final size distribution in the range 20-100 nm which has not been achieved with the $\{Sn(NMe_2)_2\}_2$ complexes. The relative similarity of the two reactions bring out a question about the reaction mechanism. Does the reaction involve intermediate species related to the amide complexes family?

To answer this question, we could consider the reactions involving a transfer of hydrides to Sn complexes, as repoerted in the literature. For instance, single-crystalline Sn nanorods are synthesized using a multistep seed-mediated method involving the reaction of $SnCl_2$ with $NaBH_4$ in tetraethylene glycol (TEG), in the presence of poly(vinylpyrrolidone) (PVP)[35,36]. An addition of

metals salts to the β-Sn seed solution yields intermetallic M-Sn (M=Co, Ni, Au, Cu, Ag, Ru, Pt) nanocrystals. In this study, the reaction mechanism of borohydrides at high temperature has not been elucidated. Since no investigation of reaction between amine-borane complexes and Sn complexes is reported in the literature, we shall compare the mechanism with other metallic systems.

On the one hand, the synthesis of Ni NPs from the reduction of $Ni(acac)_2$ with tributylamine-borane (BTB) has been reported in the presence of oleylamine and oleic acid [37]. These particles can catalyse amine-borane dehydrogenation. Following the same schema, Pd NPs for catalytic oxidation of formic acid in fuel cell conditions can be obtained by reducing $Pd(acac)_2$ with BTB in the oleylamine-mediated synthesis[38]. The AB derivative *t*-butylamine-borane complex also reduces $HAuCl_4$ in the presence of OAm to yield Au NPs[39]. Unfortunately, the very interesting results reported in the previous studies are not supported by mechanistic studies.

On the other hand, amine-borane complexes also react with amide metal-organic complexes. Diisopropylamine–borane (AeB) has been investigated as reducing agent for the synthesis of Fe NPs [40]. As proposed by the authors, the reaction between AeB and $Fe\{N(SiMe_3)_2\}_2$ complex generates diisopropylimine–borane (AoB) and H_2 which reduces $Fe\{N(SiMe_3)_2\}_2$, followed an unclear further decomposition with B incorporation in Fe NP.

The same reaction has been performed with $Co\{N(SiMe_3)_2\}_2$ and followed by reaction with a $Rh(allyl)_3$ complex [41]. The bimetallic particles are formed in a sequential manner which allows for the directed segregation of the two metallic species in the core (Fe or Co) and on the surface (Rh).

In the present research, we additionally describe the synthesis of Ni, Pd, Pt NPs, using the same synthetic pathway of metal-acetylacetonate reaction with amine-borane. This chemical route yields metallic NPs with a size suitable for catalysis (3-5 nm) in the absence of surfactants and stabilizers, i.e. with a clean surface. Our results on bimetallic Sn/Pd are consistent with the versatility of the amine-borane reduction pathway using stable metal-acetylacetonate complexes.

As exposed in the introduction, our primary goal is to circumvent the use of H_2, which poses issues of safety, by generating in-situ H_2 from the DMAB decomposition. The DMAB thermal decomposition starts at 130°C to release a hydrogen molecule and dimer structure. Our DSC measurements show a decomposition temperature of DMAB which corresponds to the release of hydrogen molecules. However, the reaction with $Sn(acac)_2$ occurs at temperature as low as 70°C .

The analysis of the ^{11}B-NMR spectra clearly shows the formation of a new species which differs from the dimer (di-borane) resulting from H_2 generation (Figure 9a). The new species displays a

peak at 18.5 ppm (^{11}B-NMR spectrum), which increases with the ratio of $Sn(acac)_2$ versus amine-borane. Since acetylacetonate is the only source of oxygen in the reaction, this peak certainly corresponds to the formation of a compound with a B-O bond which results from a reaction between the borane and acetylacetonate moieties. On Figure 9b, we propose a possible chemical pathway which accounts for the chemical reduction of Sn(II) by the hydrogen atoms of the borane and the amine, followed by the subsequent nucleophilic attack of the oxygen on the borane. The reduction mechanism goes through the formation of a cyclic intermediate. The intermediate complex coordination number increases from 4 to 6 and the coordination changes from tetragonal to octahedral. In the next step, one of the B-H bonds is released and acetylacetonate group coordinates the boron to give a possible intermediate. An additional intermediate is formed by the reaction of one more amino-borane equivalent, and subsequently forming the B-acetylacetonate bonds. This complex, presumably dioxaborine (Figure 9b), is analyzed as the only by-product by ^{11}B-NMR (singlet, 18.5 ppm).

The mechanism demonstrates the amine-borane (DMAB) coordination to the Sn(II) metal center and its reduction to yield Sn NPs. The synthetic mechanism is found to involve the reactivity of acetylacetonate ligands with borane. The chemical reduction of $Sn(acac)_2$ is a competitive reaction for the DMAB thermal decomposition and the results obtained with $Sn(hfac)_2$ strengthens this point. The reaction kinetics are greatly enhanced by the presence of electronegative CF_3 groups, showing the pivotal role of the ligands during the reaction of Sn precursors.

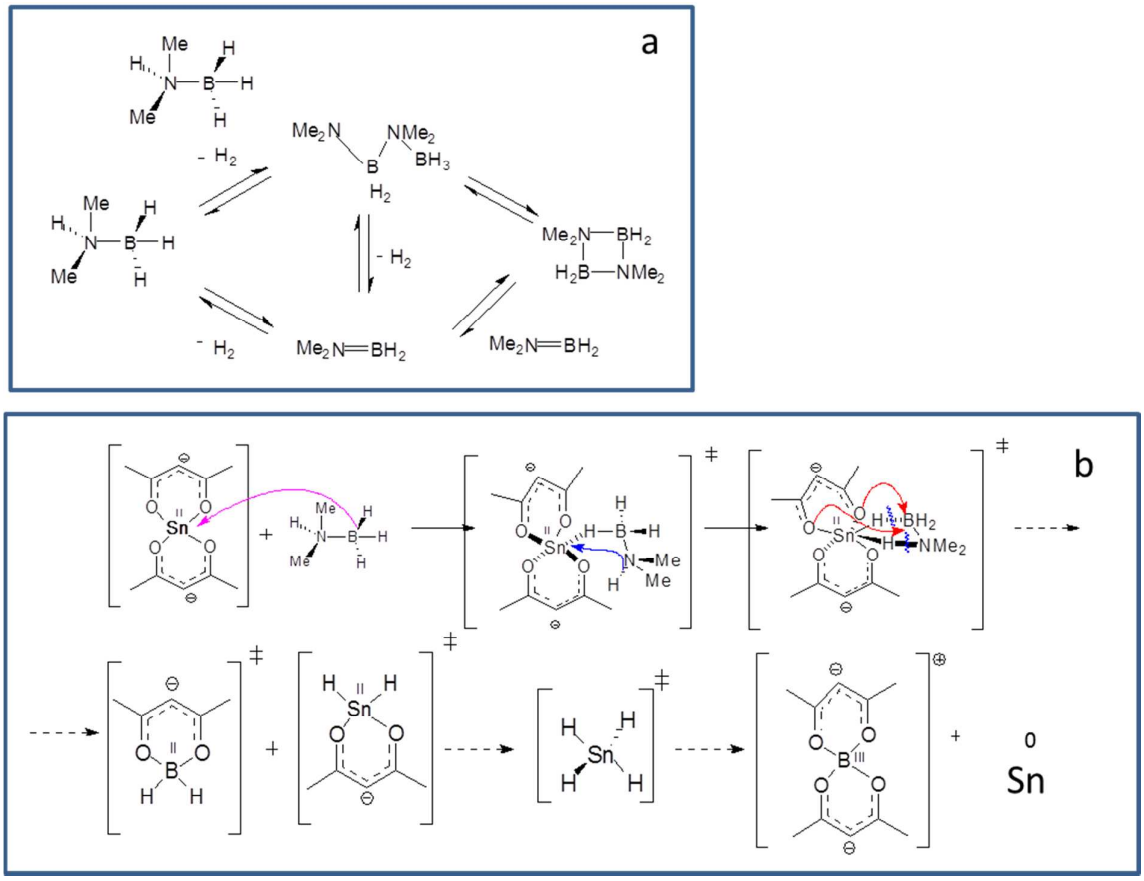

Figure 9: (a) DMAB dimerization mechanism and (b) possible reaction mechanism in the presence of $Sn(acac)_2$.

The reaction mechanism is very different from the one reported on $M\{N(SiMe_3)_2\}_2$ (M: Co or Fe) where the AB complex acts as a local source for H_2.[39,40] We believe our findings will help in the investigation of more stable acetylacetonate complexes as metal precursors for nanomaterials synthesis.

Conclusions

Sn NPs with well-defined sizes in the range 20-100 nm have been synthesized using a chemical reduction route of metal acetylacetonate by dimethylamine-borane *Lewis* complex. The reduction involves a reaction mechanism specific to acetylacetonate complexes. The use of amino-borane as reducing agent is effective for monometallic systems like Ni, Pd, Pt NPs and for mixtures like Sn/Pd NPs. Furthermore, the investigation of the mechanism, mainly by ^{11}B-NMR and calorimetry, shows a different pathway than the already reported in-situ H_2 release. The amino-borane reacts with the acetylacetonate complex to form a hydride intermediate which further yields metallic NPs.

This original pathway can be exploited and tuned by changing the nature of the ligands to enhance the kinetics of the reaction, as demonstrated with the alkyl fluorides groups. Furthermore, the advantage of this new surfactant-free synthesis is the ability to obtain metallic NPs with a clean surface, without using a gaseous H_2 source.

Experimental section

Synthesis of NPs

The NPs were synthesized using the following reagents; the Tin(II)acetylacetonate ($Sn(acac)_2$, Strem Chemicals, >98%), Tin(II)hexafluoroacetylacetonate ($Sn(hfac)_2$, Strem Chemicals, >99.9%), Borane-dimethylamine complex (DMAB, Alfa Aesor Chemicals, >97%), 1-Hexadecylamine (HDA, Acros Chemicals, >90%) and toluene (Fisher) were kept in a glove-box until use. In order to store the mesitylene (Fisher), it was degased, dried, stored on molecular sieves and kept in a glovebox. $Ni(acac)_2$, $Pd(acac)_2$, $Pt(acac)_2$ (all from Strem Chemicals, >98%), Dimethylsulfoxide (DMSO, Acros Chemicals, >99.9%) were used as received and kept in ambient atmosphere. The glovebox was used as a dry and inert atmosphere with N_2 filled, O_2< 1 ppm, H_2O< 1 ppm. Prior to use, all chemicals were flushed with nitrogen and all of the reactions were performed under an inert atmosphere.

The $Sn(acac)_2$ (0.5mmol) was stirred in a vial with 5mL mesitylene. DMAB (2 mmol) was dissolved and stirred in a vial with 5 mL mesitylene at 40°C for 10 min. A 3 neck-flask was connected to a Schlenk line and to a condenser with water stream. The flask was flushed with N_2 and the two solutions were added simultaneously by fast injection. The solution was stirred at 150°C for 2 hours under constant nitrogen bubbling. At the end of the synthesis, the dark colloidal (brown-black color) solution was left and cooled to room temperature. In order to separate the solid product, the dispersion was centrifuged at 4000 rpm for 10 min and redispersed in the same solvent (mesitylene, 2mL) this procedure was repeated three times. The cleaning procedure was followed by three washes with DMSO (dimethyl sulfoxide, 2mL) at 4000 rpm for 10 min. Finally, the obtained Sn NPs were dispersed in DMSO.

The effect of different precursor/reducing agent ratios was investigated, using the stoichiometric $Sn(acac)_2$/DMAB ratios of; 1:2 [0.5 mmol $Sn(acac)_2$, 1 mmol DMAB]; 1:4 [0.5 mmol $Sn(acac)_2$, 2 mmol DMAB]; 1:8 [0.5 mmol $Sn(acac)_2$, 4 mmol DMAB]; 1:12 [0.5 mmol $Sn(acac)_2$, 6 mmol DMAB]. The total volume of the solvent was constant at 10 ml. The solution was stirred at 150°C for 2 hours under constant nitrogen bubbling, using a 3 neck-flask.

This procedure was repeated using $Sn(hfac)_2$ instead Sn(acac)2 with the same experimental protocol with a ratio $Sn(hfac)_2$/DMAB 1:2 [0.5 mmol $Sn(hfac)_2$ and 1 mmol DMAB].

The effect of a steric surfactant was examined by using different stoichiometric ratios of hexadecylamine (HDA) and a constant quantity of DMAB [0.5mmol] and $Sn(acac)_2$ [0.25 mmol] as described for the surfactant-free reaction. The addition of 0.5 mmol and 1 mmol HDA correspond to the metal precursor/surfactant ratio of 1:2 and 1:4 respectively.

The reaction between $M(acac)_2$ (M=Ni, Pd, Pt) and DMAB was done using the previously described procedure (Synthesis of NPs). The stoichiometric precursor/reducing agent ratio was kept at 1:2. The syntheses were performed for 2 hours at 50°C under continuous stirring. The solutions were cleaned by the previously described cleaning procedure.

Analytical instruments

The synthesis mechanism was investigated by differential scanning calorimetric (DSC) technique and by nuclear magnetic resonance (NMR).

Differential scanning calorimetry (DSC) was done with a Mettler Toledo DSC-822 system equipped with a liquid nitrogen cooling system, at a heating rate of 3 °C min^{-1}, in the temperature range of 25-250 °C. The enthalpy profile of the thermal decomposition of DMAB was investigated for different stoichiometric Sn(acac)2 /DMAB ratios (1:1 ,1:2 and 1:4) in a solvent free reaction.

^{11}Boron-NMR (instrument used: Bruker Avance-400, 128.3 MHz for ^{11}B) spectra were used in order to prove the supposed mechanism. The reactions between $Sn(acac)_2$ and DMAB with 1:1 and 1:4 $Sn(acac)_2$ /DMAB ratios were investigated in a solvent-free reaction and were compared with the typical spectrum of DMAB. In addition, the ^{11}B-NMR spectra of DMAB annealed at 150 °C, 200 °C and 300 °C, under continuous stirring for 48h, were investigated. At the end of the reaction, $CDCl_3$ was added to the mixture and the filtrated supernatant was checked by NMR.

Characterization

The NPs morphology and structure were investigated by transmission electron microscopes (TEM JEOL 1400, LaB_6). The TEM observations were made by taking bright field images and selected area electron diffraction (SAED) patterns. The samples were prepared by placing a drop of a diluted solution on a 400 mesh carbon-coated copper grid. Dynamic light scattering (DLS) was measured on a Sympatek Nanophox instrument with a He−Ne laser (λ = 632.8 nm) based on photon cross-correlation spectroscopy (PCCS) in order to avoid multiple scattering. Scattering angle was set to

90° and temperature was set to 25 °C, and measurements were performed three times at two different concentrations. All hydrodynamic average diameters and polydispersity were calculated from the non-negative least-squares fitting of the autocorrelation curve using the Stokes−Einstein equation. The powder X-ray diffraction (XRD) of the metallic NPs were acquired with a Bruker AXS D8 Advance diffractometer with Cu Kα (λ = 1.5418 Å) operating at 40 kV/40 mA. Additional X-ray diffraction (XRD) measurements were performed with Rigaku SmartLab X-ray diffractometer using Cu radiation generated at 40 kV and 30 mA (CuK_{α}= 1.542 Å) as the X-ray source. The data were collected from 2θ = 20° to 90°. X-Ray Photoelectron Spetroscopy is performed with a Kratos axis HS spectrometer. Data manipulation and interpretation is carried out with OEM Vision 2 software.

Acknowledgements:

The authors thank the staff scientists from the Department of Chemistry in Bar Ilan University, especially Dr Hugo E. Gottlieb for his help for NMR, Dr Michal Afri for calorimetry, Mrs Luba Lubarka for TEM, Dr. Yehudit Grinblat for HR-TEM, Dr. Yosi Gopher for XPS, and Dr. Gili Cohen Taguri for XRD.

Bibliography

1. A. Staubitz, A. P. M. Robertson, and I. Manners, *Chem. Rev*, 2010, **110**, 4079–4124.

2. T. He, J. Wang, G. Wu, H. Kim, T. Proffen, A. Wu, W. Li, T. Liu, Z. Xiong, C. Wu, H. Chu, J. Guo, T. Autrey, T. Zhang, and P. Chen, *Chem. Eur. J.*, 2010, **16**, 12814–12817.

3. E. M. Leitao, N. E. Stubbs, A. P. M. Robertson, H. Helten, R. J. Cox, G. C. Lloyd-Jones, and I. Manners, *J. Am. Chem. Soc*, 2012, **134**, 16805–16816.

4. L. Schlapbach and A. Züttel, *Nature*, 2001, **414**, 353–358.

5. B. L. Davis, D. A. Dixon, E. B. Garner, J. C. Gordon, M. H. Matus, B. Scott, and F. H. Stephens, *Angew. Chem. Inter. Ed.*, 2009, **48**, 6812–6816.

6. V. Pons, R. T. Baker, N. K. Szymczak, D. J. Heldebrant, J. C. Linehan, M. H. Matus, D. J. Grant, and D. A. Dixon, *Chem. Commun*, 2008, 6597–6599.

7. X. Yang and M. B. Hall, *J. Am. Chem. Soc.*, 2008, **130**, 1798–1799.

8. T. J. Clark, C. A. Russell, and I. Manners, *J. Am. Chem. Soc.*, 2006, **128**, 9582–9583.

9. D. Pun, E. Lobkovsky, and P. J. Chirik, *Chem. Commun*, 2007, 3297–3299.

10. C. A. Jaska and I. Manners, *J. Am. Chem. Soc.*, 2004, **126**, 2698–2699.

11. T. M. Douglas, A. B. Chaplin, A. S. Weller, X. Yang, and M. B. Hall, *J. Am. Chem. Soc.*, 2009, **131**, 15440–15456.

12. C. A. Jaska and I. Manners, *J. Am. Chem. Soc.*, 2004, **126**, 9776–9785.

13. M. E. Sloan, T. J. Clark, and I. Manners, *Inorg. Chem.*, 2009, **48**, 2429–2435.

14. D. A. Addy, J. I. Bates, M. J. Kelly, I. M. Riddlestone, and S. Aldridge, *Organometallics*, 2013, **32**, 1583–1586.

15. M. G. Crestani, M. Muñoz-Hernández, A. Arévalo, A. Acosta-Ramírez, and J. J. García, *J. Am. Chem. Soc.*, 2005, **127**, 18066–18073.

16. Y. Luo and K. Ohno, *Organometallics*, 2007, **26**, 3597–3600.

17. M. E. Sloan, A. Staubitz, T. J. Clark, C. a Russell, G. C. Lloyd-Jones, and I. Manners, *J. Am. Chem. Soc*, 2010, **132**, 3831–3841.

18. Y. Jiang and H. Berke, *Chem. Commun*, 2007, 3571–3573.

19. M. Rosello-Merino, J. Lopez-Serrano, S. Conejero, M. Roselló-Merino, J. López-Serrano, and S. Conejero, *J. Am. Chem. Soc.*, 2013, **135**, 10910–10913.

20. L. Euzenat, D. Horhant, Y. Ribourdouille, C. Duriez, G. Alcaraz, and M. Vaultier, *Chem. Commun.*, 2003, 2280–2281.

21. M. C. Denney, V. Pons, T. J. Hebden, D. M. Heinekey, and K. I. Goldberg, *J. Am. Chem. Soc*, 2006, **128**, 12048–12049.

22. T. J. Hebden, M. C. Denney, V. Pons, P. M. B. Piccoli, T. F. Koetzle, A. J. Schultz, W. Kaminsky, K. I. Goldberg, and D. M. Heinekey, *J. Am. Chem. Soc.*, 2008, **130**, 10812–10820.

23. K. Soulantica, A. Maisonnat, M.-C. Fromen, M.-J. Casanove, and B. Chaudret, *Angew. Chem. Inter. Ed.*, 2003, **42**, 1945–1949.

24. E. J. H. Lee, C. Ribeiro, E. Longo, and E. R. Leite, *J. Phys. Chem*, 2005, **109**, 20842–20846.

25. A. K. Sinha, M. Pradhan, S. Sarkar, and T. Pal, *Environ. Sci. Technol*, 2013, **47**, 2339–2345.

26. K. Kravchyk, L. Protesescu, M. I. Bodnarchuk, F. Krumeich, M. Yarema, M. Walter, C. Guntlin, and M. V. Kovalenko, *J. Am. Chem. Soc.*, 2013, **135**, 4199–4202.

27. M. Alaf and H. Akbulut, *J. Power Sources*, 2014, **247**, 692–702.

28. S. Hermanek, *Chem. Rev*, 1992, **92**, 325–362.

29. A. Staubitz, A. P. M. Robertson, M. E. Sloan, and I. Manners, *Chem. Rev.*, 2010, **110**, 4023–4078.

30. R. A. Geanangel and W. W. Wenedlant, *Thermochim. Acta.*, 1985, **86**, 375–378.

31. D. J. Grant, M. H. Matus, K. D. Anderson, D. M. Camaioni, S. R. Neufeldt, C. F. Lane, and D. a Dixon, *J. Phys. Chem. A*, 2009, **113**, 6121–6132.

32. J. Fabian and H. Hartmann, *J. Phys. Org. Chem.*, 2004, **17**, 359–369.

33. C. Nayral, E. Viala, P. Fau, F. Senocq, J. C. Jumas, A. Maisonnat, and B. Chaudret, *Chem. Eur. J.*, 2000, **6**, 4082–4090.

34. C. Nayral, T. Ould-Ely, A. Maisonnat, B. Chaudret, P. Fau, L. Lescouzères, and A. Peyre-Lavigne, *Adv. Mater.*, 1999, **11**, 61.

35. N. H. Chou and R. E. Schaak, *Chem. Mater.*, 2008, **20**, 2081–2085.

36. N. H. Chou and R. E. Schaak, *J. Am. Chem. Soc.*, 2007, **129**, 7339–7345.

37. O. Metin, V. Mazumder, S. Ozkar, and S. Sun, *J. Am. Chem. Soc.*, 2010, **123**, 1468–1469.

38. V. Mazumder and S. Sun, *J. Am. Chem. Soc.*, 2009, **131**, 4588–4589.

39. S. Peng, Y. Lee, C. Wang, H. Yin, S. Dai, and S. Sun, *Nano Res.*, 2008, **1**, 229–234.

40. F. Pelletier, D. Ciuculescu, J. G. Mattei, P. Lecante, M. J. Casanove, N. Yaacoub, J. M. Greneche, C. Schmitz-Antoniak, and C. Amiens, *Chem. Eur. J.*, 2013, **19**, 6021–6026.

41. N. Atamena, D. Ciuculescu, G. Alcaraz, A. Smekhova, F. Wilhelm, A. Rogalev, B. Chaudret, P. Lecante, R. E. Benfield, and C. Amiens, *Chem. Commun.*, 2010, **46**, 2453–5.